SUSAN C. LEE, DONALD E. MAURER, and KEITH L. MUSSER

PREDICTING CLUTTER DURING ANOMALOUS PROPAGATION CONDITIONS

Excessive clutter caused by anomalous propagation conditions severely degrades radar performance in many regions of the world. This article describes methods that can be used to predict anomalous clutter amplitude for site-specific radar parameters, terrain features, and atmospheric conditions and to predict the effects of radar Doppler processing on evaporation-ducted sea clutter.

INTRODUCTION

Under anomalous propagation conditions, ground and sea clutter can be caused by superrefraction (when rays are bent down with a radius of curvature approaching that of the earth) and by ducting (when rays are bent down with a radius of curvature much less than the radius of the earth). Because of this diversion of energy toward the surface, a radar may detect returns from objects that would normally be well below the radar horizon, including ground and sea returns. Often, clutter-mitigation techniques are not applied at these extreme ranges, and targets may be obscured. Further, the anomalous clutter returns can be much larger than expected, since, under ducting conditions, the two-way propagation loss can be much less than the usual $1/R^4$ (because the duct confines the rays and does not allow spherical spreading, the loss is typically nearer $1/R^2$, where R is range). Finally, the spectrum of anomalous sea clutter may be quite different from that of normal sea clutter, so that the combination of normal MTI (moving target indicator) and Doppler processing is ineffective for discriminating targets from false alarms. Because of these effects, the radar design principles used for sensitivity time control and for MTI and Doppler filter weights are significantly affected by the anomalous propagation phenomenon.

Two computer simulation tools have been developed to predict and understand clutter better under anomalous propagation conditions: The clutter amplitude model maps the location and strength of clutter returns under various atmospheric conditions; the clutter spectrum model computes a simulated clutter return to be used as input to various radar models analyzing the effect of typical Doppler and MTI processing on sea clutter returns induced by anomalous propagation.

CLUTTER AMPLITUDE MODEL

Clutter maps provide the geographic distribution of clutter returns within the unambiguous range of the radar. When predicted clutter is displayed in the plan position indicator format, a radar designer can decide what range intervals require clutter mitigation, and a radar observer can recognize clutter features induced by anomalous propagation.

Prediction of clutter induced by anomalous propagation requires new information not usually considered in the normal understanding of clutter:

1. Two-way propagation loss is not necessarily proportional to $1/R^4$; loss must be determined for the specific atmospheric conditions.
2. Geographic regions not normally illuminated because of terrain- or horizon-masking may be illuminated by ducted energy.
3. The surface incidence angle is not simply determined from the ray launch angle; instead, it is a function of launch angle and the propagation path.
4. The angular dependence of normalized radar cross sections of ground and sea at very shallow incidence angles must be considered.

Clutter maps are produced by combining environmental data with the outputs of three major simulation programs. First, the EMPE (Electromagnetic Parabolic Equation)[1,2] simulation produces a file of one-way transmission losses at each height and range in the entire radar coverage area. The code performs a physical optics calculation of the propagation loss under anomalous propagation conditions. It gives the spatial distribution of energy radiated by the antenna into both vertically and horizontally inhomogeneous refractive layers. The effects of diffraction and sensitivity to wavelength and phase are included.

Next, the Raytrace[3] simulation calculates the grazing angle and location (latitude, longitude, and elevation) of rays that strike the surface. This code is a geometrical optics simulation that solves equations based on Fermat's principle to describe ray paths. Figure 1 illustrates the similarities and the differences between the output displays of (a) EMPE and (b) Raytrace for the same surface-ducting conditions. Raytrace clearly shows rays hitting the surface at multiple range intervals, while EMPE gives the propagation loss at these same ranges. Generally, areas where Raytrace predicts high ray densities correspond to areas where EMPE predicts lower propagation losses.

The third simulation program uses the outputs of EMPE and Raytrace. The one-way transmission loss at

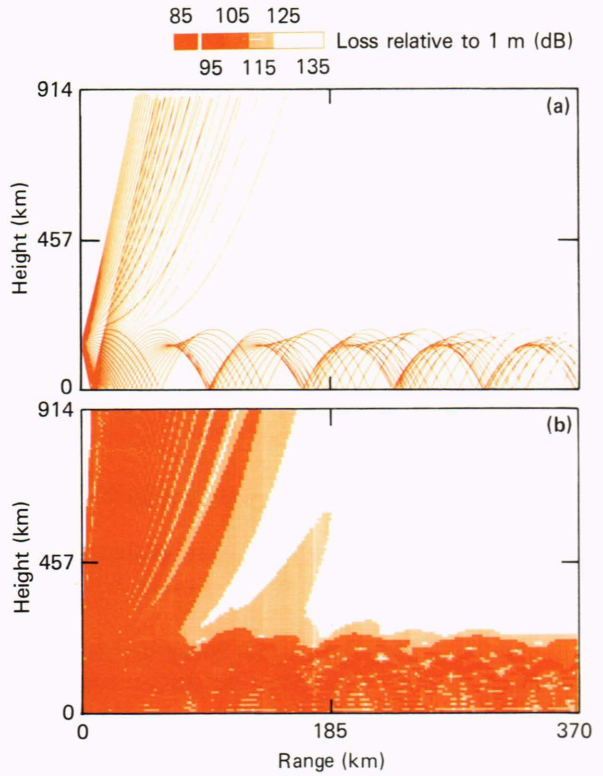

Figure 1—(a) EMPE coverage plot and (b) Raytrace plot for the same surface-ducting conditions.

each location where Raytrace predicts that a ray will strike the surface is "looked up" in the file produced by EMPE. From this information and other Raytrace outputs, the clutter simulation program calculates the clutter return.

Four types of input data are required:

1. *Radar parameters:* The parameters used to describe the radar are antenna height above ground, frequency, beam width, angle of the beam from the horizontal, and compressed pulse width.
2. *Refractivity profile:* This input describes the vertical profile of the atmosphere's refractivity. The Raytrace simulation limits the clutter calculation to only one profile per run. Thus, the atmospheric model is vertically inhomogeneous and horizontally homogeneous.
3. *Surface elevation:* The surface elevation data can be modeled (for test purposes or for making parametric studies) or can be read from a file of actual terrain elevation at a particular site.
4. *Surface type and roughness:* The surface type and roughness are derived from the elevation data. If the elevation is greater than zero (i.e., above sea level), the surface is assumed to be sand. Otherwise, the surface is assumed to be seawater (with 1-m waves). These choices reflect the terrain expected at the site first studied using this technique; other terrain types and sea states could be incorporated as needed.

The radar parameters and the refractivity profile are inputs to the EMPE simulation. Each run produces a "slice" through the antenna pattern at one azimuth (see Fig. 1a). Although EMPE incorporates horizontal inhomogeneity of refractivity, the overall clutter simulation is limited by Raytrace to one refractive profile per run. EMPE does not incorporate surface features (i.e., it assumes that the earth's surface is at sea level everywhere). Thus, EMPE runs are azimuthally symmetric, and one run is used to predict propagation loss in all directions. The assumption of a smooth earth limits the accuracy of the clutter model, since EMPE ignores the exact surface roughness and terrain shadowing imposed by the actual terrain. However, the resulting inaccuracy is slight in the overall dynamic range prediction of the clutter amplitude, because almost all the loss is along the two-way path between the antenna and the surface, and not along the small excursions of the surface.

Inputs to the Raytrace simulation are the radar parameters, the refractivity profile, and the surface elevation data. At the end of each integration step in the ray path calculation, the ray height is checked against the terrain height at that range. If the ray is below the surface, the simulation "backs up" to the preceding step and uses an interpolative procedure to find the exact range at which the ray struck the ground. The range and height at which rays strike the ground are input to the clutter simulation.

Raytrace assumes that all changes in elevation occur in a stepwise fashion. By examining the endpoints of the ray-trace step that hits the ground, Raytrace can determine whether the ray hit a "horizontal" segment or a vertical "wall" between segments. Rays that hit a horizontal segment are reflected at an angle (from the horizontal) equal to the incidence angle. Rays that hit a wall are terminated. The clutter return is calculated identically, as described below, for ray hits on both horizontal segments and walls.

Raytrace also produces the ray incidence angle or grazing angle of rays that strike the ground. The grazing angle is defined as the angle between the ray and a tangent to the earth's surface. Although the simulation can compute the angle between the horizontal and each ray, the slope of the ground is not known. To compute clutter, the ground is always assumed to be flat wherever the rays strike. This makes it easy to calculate the grazing angle, and introduces no more error than any other assumption.

Since the terrain profile is potentially different in each azimuthal direction, a Raytrace simulation result depends on azimuthal direction. To produce the clutter maps, ray traces are calculated for azimuths from 0 to 360°, at 1° intervals. At each azimuth, 50 rays are traced, launched at evenly spaced intervals between 0.25 and −0.25° of elevation.

After EMPE and Raytrace have produced their outputs, the clutter return calculation is straightforward. First, on the basis of the surface type and the grazing angle (produced by Raytrace), the normalized radar cross section of the ground is interpolated from a look-up table of values. The values were digitized by hand from graphs of empirical scattering data[4] for "Arizona desert" and "sea clutter – 1-m waves" (S-band, horizontal-horizontal

polarization). Where necessary, the normalized radar-cross-section graphs were extrapolated to cover small grazing angles.

The clutter return itself, CR (in decibels), is

$$CR = 2TL + \log\left(\frac{c\tau R\theta \sec\varphi}{2}\right) + \sigma_0(\varphi) ,$$

as formulated in Ref. 5, where

σ_0 = normalized radar cross section of the surface (dB),
c = speed of light (m/μs),
τ = compressed pulse width (μs),
R = range (m),
θ = beam width (rad),
φ = grazing angle (rad),
TL = one-way transmission loss (dB).

The clutter return is calculated only for locations where Raytrace predicts that rays will strike the ground, since no surface clutter is expected otherwise. Where rays do strike the ground, EMPE predicts the energy loss from the antenna to that point. If the ground were a perfect reflector, twice that energy loss would be expected for the round-trip back to the antenna. Some energy is lost by surface scattering, however; this is taken into account by multiplying the radar cross section of the ground by the area of the ground illuminated by the radar.

The clutter returns, as displayed on a simulated plan position indicator display, make up what is called a clutter map. The strength of the clutter return is indicated by the color in which it is displayed. The color bar can be used to assign an amplitude to each color, in decibels relative to the transmitter power at 1 m. To orient the viewer, approximate coastline locations can be superimposed on the display.

Raytrace predicts the path of a beam consisting of 50 discrete rays pointed around 360° of azimuth at 1° increments. Each ray that strikes the ground is assumed to cover some spatial extent in azimuth (±0.5°) and range (calculated from the compressed pulse width). All display pixels that cover this area are colored to represent the clutter return calculated for that ray.

Because of the many sources of unquantifiable error (e.g., grazing-angle uncertainties, extrapolated radar-cross-section data, and smooth-earth EMPE transmission-loss predictions used over a rough terrain), these numerical results give a qualitative, rather than quantitative, picture of the clutter caused by anomalous propagation. The maps are most accurate over the ocean, where assumptions made in the model are most nearly correct. Despite the numerous deficiencies in the model, the resultant clutter maps compare well with actual plan position indicator displays of anomalous clutter, when site-specific clutter maps are made. No other method exists to provide the radar designer this dynamic range of clutter amplitude under anomalous propagation conditions.

The output of the clutter map simulation can be made site-specific by using radar parameters, refractivity profiles, and terrain elevation maps from a particular site. In Figs. 2 to 4, a radar plan position indicator is simulated at a site near a gulf coast. The unambiguous range in the display is 370 km; the gulf is 278 to 315 km wide. Table 1 lists radar parameters chosen to simulate the radar. Statistics have been compiled on refractivity profiles taken twice daily for this site during 1978 and 1979.[6] The superrefractive and ducting conditions used in generating Figs. 2 to 4 are quite typical of the area; during some months, these conditions are present on 70% of the days. A computer-readable file of terrain elevation data is available for most of the peninsula, on a grid of 5′ (latitude) by 5′ (longitude). This coarse terrain map limits the scale of the clutter features predicted by the clutter map model.

Figure 2 is a predictive clutter map during superrefraction; clutter is mainly confined to the rising ground inland of the radar and to the mountains of the coast across the gulf, normally well below the radar horizon. Figure 3 shows predictive clutter caused by an elevated duct. A "clutter ring" is formed where the duct brings energy to the surface; scattering of this energy inland of the radar causes diffuse clutter throughout the radar range. Figure 4 predicts an extreme case of clutter caused

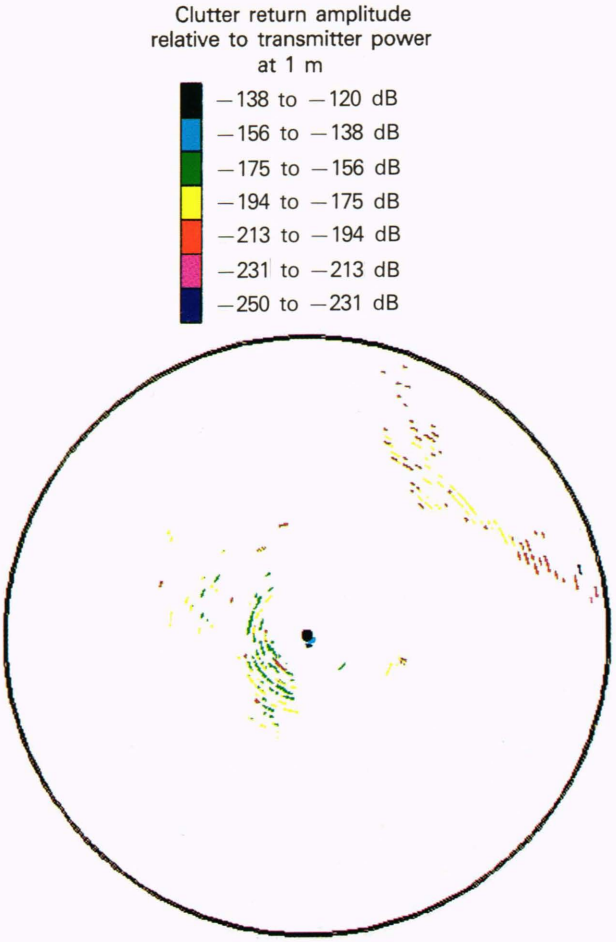

Figure 2—Simulation map of clutter caused by anomalous propagation during superrefractive conditions at a gulf site.

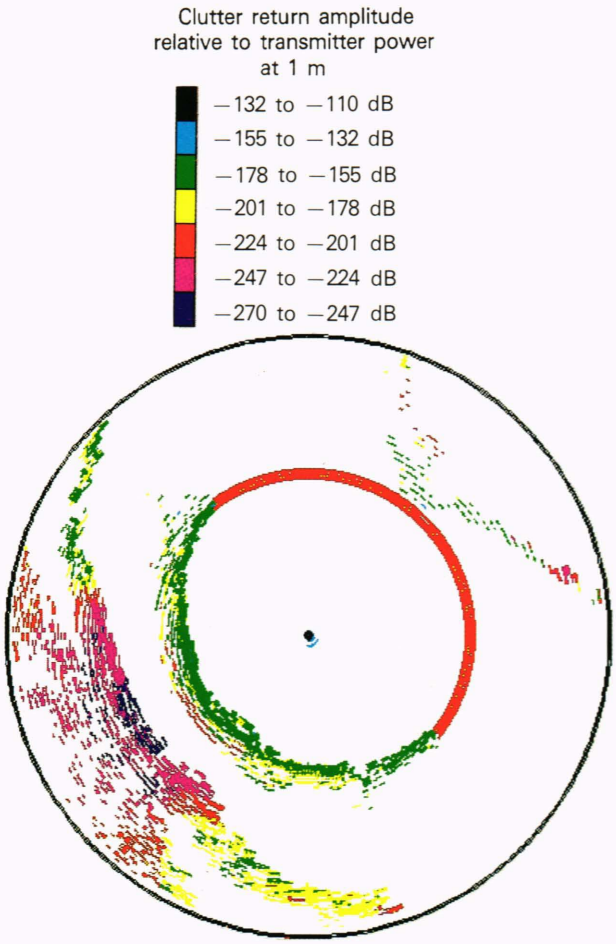

Figure 3—Simulation map of clutter caused by anomalous propagation during elevated ducting conditions at a gulf site.

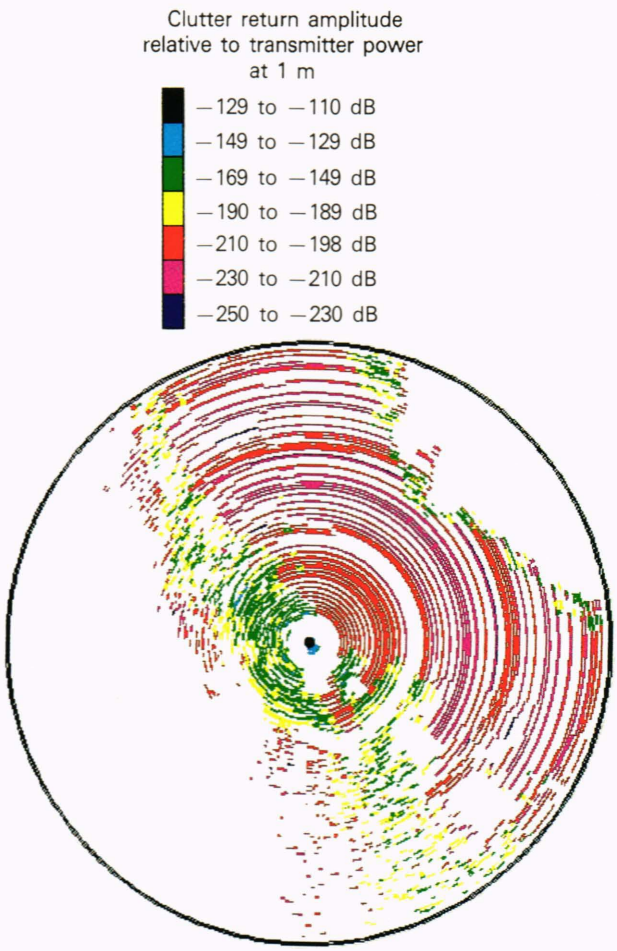

Figure 4—Simulation map of clutter caused by anomalous propagation during elevated ducting conditions at a gulf site.

Table 1—Radar parameters.

Antenna height above sea level	137 m
Frequency	1215 MHz
Horizontal and vertical beam width	2°
Angle of beam from horizontal	0.0°
Compressed pulse width	1.5 μs

by a surface duct. Numerous clutter rings are caused by energy bouncing in the duct. For comparison, Fig. 5 is a photograph of a plan position indicator display from a real radar at the gulf site, showing clutter typical of surface-ducting conditions. Many features on the simulated clutter map, such as clutter rings over the ocean and land mass outlines (particularly the coastal mountains, well below the radar horizon), are seen on the actual plan position indicator display.

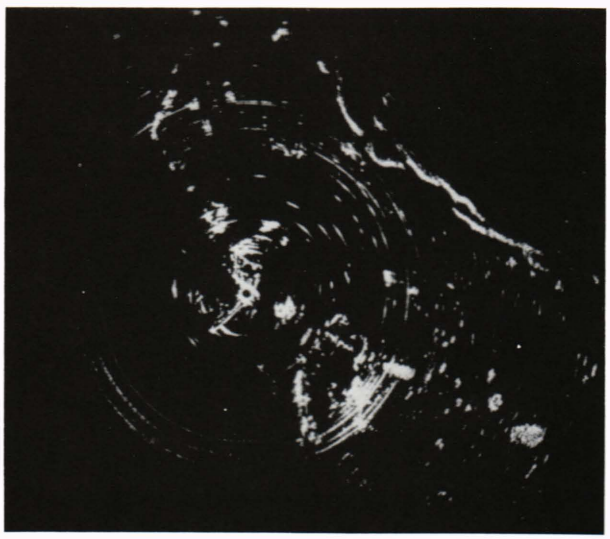

Figure 5—Plan position indicator display photographed at the gulf site simulated in Figs. 2, 3, and 4.

CLUTTER SPECTRUM MODEL

The Doppler spectrum is the Fourier transform of a time series of radar returns from each range. If the transmitted signal is $u(t)$, the return from a single target will be $Au(t - t_d)$, where A is an amplitude and t_d is a time delay. Doppler radars take advantage of the fact that the return from a moving target has a time delay

that is a function of time. The Doppler spectrum of such a signal is the Fourier transform of the transmitted signal shifted in frequency by an amount directly proportional to the velocity of the target. Any mechanism that introduces additional modulation of t_d or A into the return signal can further shift and spread the Doppler spectrum.

Anomalous propagation could introduce such amplitude time-delay modulations. One possible mechanism is limiting by the radar's analog processing. Many radars apply gain as a function of range, to avoid saturating the electronics with returns from nearby targets, while retaining sensitivity to distant targets. In a surface duct, however, radar energy can fall off as $1/R^2$, rather than $1/R^4$. The range/gain schedule used under normal conditions for the sensitivity time control may be inadequate for ducting conditions. Limiting the return introduces an amplitude modulation that could spread the Doppler spectrum.

Another mechanism is illustrated in Fig. 6, which shows what happens when a ray in a surface duct hits the ocean. Backscattered energy can return to the radar over many different paths, depending on the angle of reflection. If the angle of reflection is less than some critical angle (a function of the duct parameters), energy may also be scattered forward to a second bounce point. The location of the second bounce point is sensitive to extremely small changes in the angle of reflection at the first bounce point. For example, changing the angle of reflection from 0.300 to 0.305° changes the location of the second bounce point by 1.3 km. Thus, the moving ocean surface, by changing the angle of reflection slightly over the period of the radar transmission, could create returns from the second bounce point that erroneously indicate a target moving at high velocity. An equivalent point of view is that the intensity of radar energy illuminating a range cell at the second bounce will fluctuate as the distribution of forward-scattered energy is modulated by wave motion of the first bounce point.

Two computer simulation tools have been used to investigate the Doppler spectrum of clutter caused by anomalous propagation: an anomalous-propagation ocean-return model and a radar processing simulation. Figure 7 shows how these independent models interact.

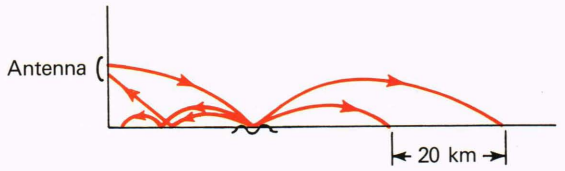

Figure 6—Possible paths followed by a ray bouncing in a surface duct, illustrating ray-path fluctuations at downrange bounce points caused by ocean surface motion.

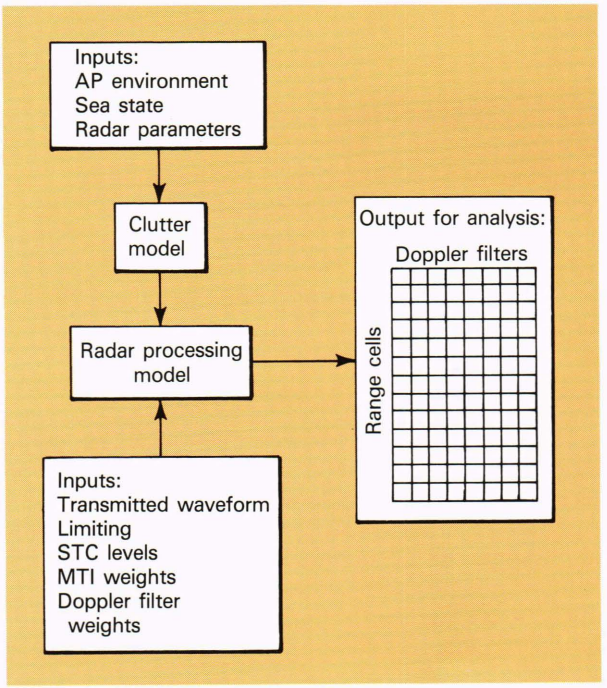

Figure 7—Block diagram showing interaction between an ocean model and a Doppler processing simulation. (AP = anomalous propagation; STC = sensitivity time control.)

OCEAN-RETURN MODEL

The transmitted signal is represented as propagating along a series of discrete rays, equally spaced over the radar beam width. A simulated clutter time-series is calculated by tracing each radar pulse along the individual ray trajectories (determined by radar, duct, and ocean surface parameters) and, at the bounce points, determining the backscattered energy. Each clutter sample is a complex number that represents in-phase and quadrature components, and consists of all individual ray contributions that arrive at the receiver at the sample time.

The amplitude of the backscatter is estimated using cylindrical attenuation and a standard radar backscatter coefficient. The round-trip time delay of the return to the antenna is taken to be twice the time of the trip out to the surface. Ray-trace simulations have shown that this delay is independent of the return path. If the angle of reflection of the ray at the surface is such that the ray will propagate forward in the duct, the ray is traced to a second bounce point. Here, the ray/surface interaction is not modeled, but a return amplitude is calculated as before. Again, the time delay of the return is taken to be twice the time to the second bounce point. The clutter is calculated at the discrete times corresponding to the radar processing sample rate.

To determine the ray/surface interactions at the first bounce point, the ocean surface height, $z = F(x,t)$, where x is range and t is time, was modeled as a zero-mean Gaussian process.[7] To complete the statistical description of this wave-height process, the autocorrelation function, $R(\rho,\tau)$, where ρ and τ are the spatial and temporal lags, respectively, must be specified. Reference 8 gives the following analytical form as a good match to measured temporal correlations:

$$R(\rho,\tau) = \alpha^2 \exp(-\rho/\lambda - \tau/T) \cos(P\rho - F\tau),$$

where

α = rms wave height,
λ = spatial correlation length,
T = correlation time,
P = dominant wave number,
F = dominant wave frequency.

This correlation function has also been compared to wave number spectra reported in Ref. 9, with good matches for wind speeds between 3.5 and 7.4 m/s. The following correlation function parameters were used in the ocean-return model simulation: $\alpha = 0.064$ m, $\eta = 3.0$ m, $T = 2$ s, $P = 3.14\ \text{m}^{-1}$, and $F = 3.59\ \text{s}^{-1}$. They correspond to a low-sea-state ocean with a significant wave height of 0.25 m and a phase velocity of 1.42 m/s for an L-band radar; this gives ocean-induced Doppler frequencies of 8 to 12 Hz.

Extending a procedure developed by Northam,[10] this stochastic model of the ocean surface is used to generate a spatially correlated sequence of wave heights downrange from the radar. Two time-correlated realizations are generated at the beginning and end of each Doppler dwell period. Surface motions during the dwell period are interpolated between the two realizations.

THE RADAR PROCESSING MODEL

Figure 8 is a block diagram of the elements in the radar processing simulation of a radar with MTI and Doppler processing. The simulation accepts the clutter return from each transmitted linear-frequency-modulated pulse as a complex-number (in-phase and quadrature components) time series with successive elements separated by about 1 μs. The clutter time series is read from a file produced independently of the radar processing model. A "pulse train" of 10 pulses is "transmitted" and processed to obtain one 8-filter Doppler output at each desired range interval.

Since the simulation is digital, all analog processing must be modeled. The antenna subsystem, the sensitivity time control, and the final receiver are all modeled as linear gains applied to the radar returns. The gain set by the sensitivity time control is a function of range.

In a radar system, the purpose of the preprocessor/modulator is to shift the radio-frequency returns to baseband and to split the signal into its in-phase (I) and quadrature (Q) components. These steps are unnecessary in the processing simulation, since the returns are generated as complex numbers (I,Q) and are already sampled at the baseband frequency. However, to evaluate the effects of limiting the radar returns, the preprocessor is assumed to be the first analog stage to saturate. Although limiting might occur anywhere in the analog processing, the choice of the preprocessor will not affect the results, since phase is preserved in the limiting process.[11] As the amplitude of the return becomes large compared with the limit level, L, the amplitude of the output approaches $4\pi/L$ for both hard and soft limiters.[11] In the processing simulation, the preprocessor demodulator is modeled by a hard limiter at $4\pi/L$. To complete the analog processing, 12-bit analog-to-digital (A/D) converters are modeled as a linear scale factor.

The first stage of digital processing is the MTI processing. The simulation uses a sliding-window, three-pulse MTI with nominal weights. Implementation of the MTI filter requires the simulation to save the output of the analog processing steps for the three most recent pulse repetition periods. Following the MTI is a rescaler, which reduces the dynamic range of the returns.

The rescaled output is input to the pulse compressor. Although the transmitted signal is assumed to be linear frequency modulation, the modeled pulse compression filter has a stepped frequency modulation impulse response. The impulse response lasts 64 samples and is grouped into eight constant-frequency steps.

Because of the imperfect match between the linear frequency modulation pulse and the pulse compressor, a pair of range sidelobes appears in the compressor output. These are suppressed by a transverse equalizer and

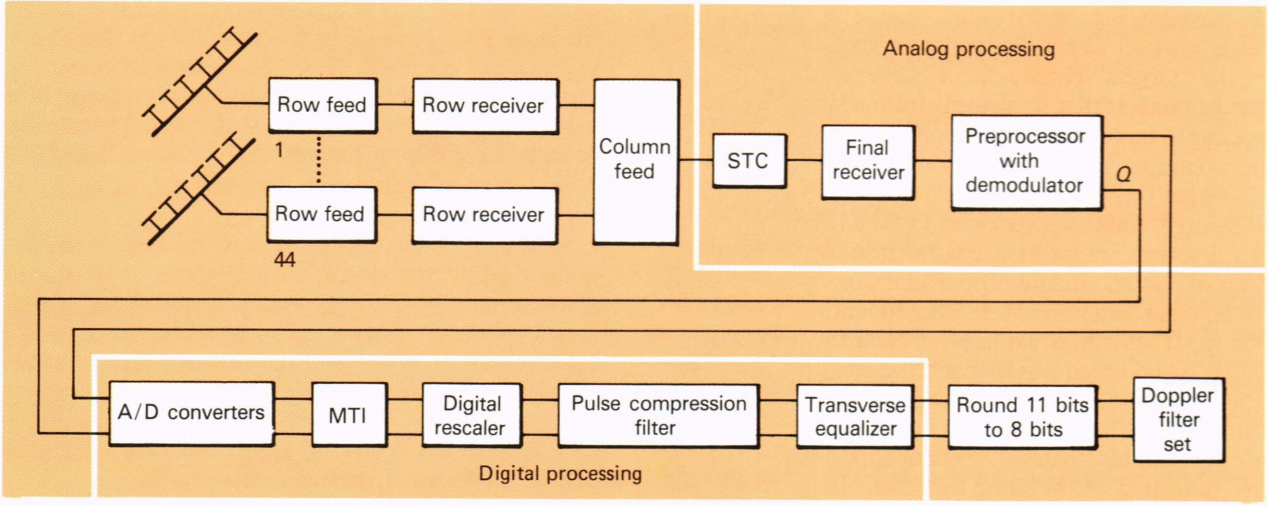

Figure 8—Block diagram of a radar processing simulation.

a Taylor weighting filter. A multiplicative factor is applied to give unity noise gain.

The Doppler filter is implemented as an 8-point discrete Fourier transform of the output of the MTI. The transform is followed by a division by $1/\sqrt{8}$ to normalize to unity noise gain. The outputs of the Doppler filters as functions of range can be printed in a table (see Table 2) or written to a file for further processing. Each of the filters is separated by 94 Hz (11.7 m/s); the filters have been arranged so that filter zero is centered on 0 Hz. Doppler frequencies outside the range of this filter bank will alias into one of the filter outputs.

CLUTTER MODELING RESULTS

To evaluate the effect of these processing steps on returns limited in the preprocessor, an 8000-point time series was generated. The spectrum of this series was flat at the level C between ± 15 Hz and zero elsewhere, representing a worst-case sea clutter spectrum. The 8000 points were processed as if they were returns from one range, producing 800 outputs from each of the eight Doppler filters. The mean and standard deviation of the output of each filter were calculated. The mean and standard deviation of the output from all filters increased when the input was limited at the level L. Figure 9 illustrates the effect of this increase of C/L from zero to 30 dB on the probability distribution function $p(x)$ of the filter outputs; clearly, for any given threshold, limiting the return at the input will increase the probability of false alarm.

The radar processing simulation has also been applied to the output of the ocean-return simulation. Ocean returns have been simulated for both standard atmospheric conditions and surface ducts. Table 2 shows some outputs of the Doppler filters for standard conditions, where the beam was pointed downward somewhat, so that the surface could be illuminated. As expected, most of the returns fall in the zero Doppler filter (± 5.8 m/s), with some overlap into adjacent filters because of the large Doppler filter sidelobes. In contrast, Table 3 shows simulated Doppler output from a bounce point for energy traveling in a surface duct. Large returns are scattered over all filters; the apparent speed and direction of the "targets" change radically over short ranges. The model predicts that sea returns from a surface duct may appear to have "speeds" comparable to those of air targets, causing false alarms.

Actual Doppler data with this appearance have been measured; Table 4 is the output of the Doppler filters of a microwave radar at a coastal near-Arctic site. It is known that anomalous propagation conditions prevailed when these data were taken, since mountains well beyond the radar horizon could be seen. Near the vicinity of the radar, wind speed was low and the sea state calm (as in the modeled ocean); evaporation (surface) ducts will not form unless these calm conditions prevail. Only sea/ice clutter had this "patchy" spectral appearance; land clutter measured at the same time had the expected nonspread spectral characteristics. Further, Doppler spreading was not observed in all directions over the ocean. Our model predicts that the occurrence of spreading is sensitive to wave slope (and thus wind direction) and should not occur at every azimuth.

Table 2—Simulated Doppler output for standard atmosphere.

	Doppler Filter Output (Hz) (equivalent speed, m/s)						
Range (km)	*−281 (−35)*	*−187 (−23)*	*−94 (−12)*	*0 (0)*	*94 (12)*	*187 (23)*	*281 (35)*
4.437	0.8	2.1	0.4	11.7	3.8	2.5	1.2
4.678	1.8	3.0	2.2	26.5	6.3	2.7	2.0
4.917	3.0	5.5	5.5	46.7	11.2	3.5	3.9
5.158	4.1	5.7	6.4	53.3	12.7	4.9	3.9
5.399	3.7	3.1	4.8	34.0	9.9	2.2	2.3
5.637	2.2	2.1	2.0	19.0	5.2	0.8	1.6

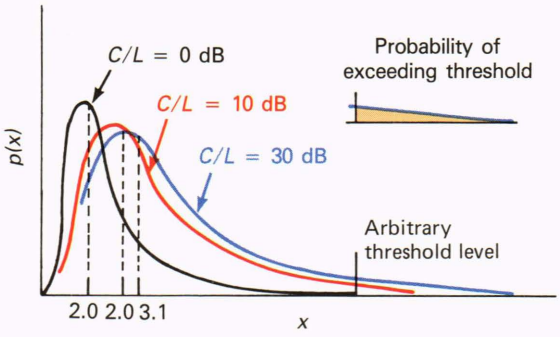

Figure 9—Effect of limiting on the probability of false alarm for clutter-to-limit ratios (C/L) of 0, 10, and 30 dB.

The clutter simulation model produces results that appear qualitatively very similar to the measured data. While encouraging, that does not establish the cause of Doppler spread during anomalous propagation. Unfortunately, very little data currently exist on the Doppler spectrum of sea clutter during anomalous propagation conditions; radar measurements are seldom accompanied by the atmospheric data needed in anomalous propagation modeling. When opportunities arise to obtain more and better data, the model can be used to plan test scenarios, to either validate or disprove the hypothesized mechanism.

SUMMARY

Anomalous atmospheric conditions can strongly affect radar clutter and clutter processing. Increased clutter amplitude and ground or sea clutter at long ranges are common. If these effects are not anticipated, sensitivity time control schedules may be set incorrectly, and clutter-mitigation techniques such as MTI and Doppler may not be used at the ranges where clutter appears. Further, anomalous propagation may change the character of the clutter return, making ineffective the use of MTIs and Doppler filters that are tuned for normal clutter.

Table 3—Simulated Doppler output for the second bounce point in a surface duct.

	Doppler Filter Output (Hz) (equivalent speed, m/s)						
Range (km)	*−281 (−35)*	*−187 (−23)*	*−94 (−12)*	*0 (0)*	*94 (12)*	*187 (23)*	*281 (35)*
73.289	10.8	8.2	3.1	9.0	3.5	8.6	13.5
73.408	7.6	3.2	6.6	7.5	5.4	6.9	15.2
73.528	9.4	5.5	9.9	5.1	8.8	4.6	10.6
73.648	9.2	8.6	5.8	6.0	7.5	4.0	10.1
73.769	10.1	7.4	4.9	5.0	6.5	0.7	4.9
73.837	16.5	9.4	3.2	2.5	2.7	9.2	11.0
74.008	21.9	7.0	4.6	2.2	1.0	17.1	28.6
74.128	28.3	4.9	7.0	3.4	5.6	20.4	29.4
74.249	21.8	5.0	4.8	3.5	9.9	10.9	16.3
74.293	10.1	4.0	4.3	3.9	5.9	1.8	11.4
74.487	12.3	6.9	10.4	1.0	7.2	15.5	29.0
74.608	27.0	17.5	14.9	9.5	7.9	24.2	39.2
74.628	18.0	13.2	12.7	13.7	6.8	19.9	16.2
74.849	7.9	7.9	4.6	7.4	5.4	6.8	6.3
74.967	7.0	4.6	2.9	2.0	7.7	5.2	7.2
75.087	15.4	11.1	6.7	6.0	7.7	14.3	16.9
75.208	34.8	22.8	6.2	5.0	12.6	27.2	32.3
75.328	23.2	16.5	6.0	3.3	5.6	13.4	11.1
75.447	9.0	3.9	4.9	2.5	6.6	2.6	11.5
75.567	3.8	3.3	5.1	1.9	3.9	1.2	10.5
75.688	0.3	1.9	1.3	4.8	8.8	6.3	7.4
75.808	2.1	5.8	4.5	7.9	6.9	7.2	9.4
75.926	0.1	6.1	6.8	7.1	4.4	2.5	4.9

Table 4—Measured Doppler output at a near-Arctic site.

	Doppler Filter Output (Hz) (equivalent speed, m/s)						
Range (km)	*−281 (−35)*	*−187 (−23)*	*−94 (−12)*	*0 (0)*	*94 (12)*	*187 (23)*	*281 (35)*
24.887	6.8	16.6	15.2	9.3	9.1	6.8	5.2
25.002	5.9	10.0	12.0	8.6	7.7	7.1	5.6
25.119	4.4	5.9	9.2	9.4	7.5	5.9	4.1
25.234	4.7	7.3	8.6	7.7	5.6	7.6	3.9
25.350	6.9	12.9	13.9	9.3	7.1	7.4	5.4
25.465	7.6	19.5	16.7	8.7	9.1	7.7	5.3
25.582	10.4	23.8	19.1	8.4	8.3	6.2	5.4
25.697	6.8	16.3	15.5	8.9	8.5	7.7	4.0
25.813	7.0	7.6	8.7	8.9	10.1	9.7	6.8
25.928	5.5	7.7	10.4	10.4	8.7	8.2	4.9
26.045	6.2	7.9	9.6	9.3	8.6	6.0	4.1
26.160	7.5	11.5	11.5	12.7	14.8	9.9	4.7
26.276	10.0	25.7	18.7	15.7	29.8	22.2	6.2
26.391	13.2	32.6	25.9	16.4	33.8	24.9	6.0
26.508	9.7	22.6	19.6	13.4	21.1	15.7	5.9
26.623	6.2	11.0	14.0	12.3	11.9	9.9	4.8
26.739	5.5	8.8	10.4	10.6	8.9	7.6	5.4
26.854	5.7	6.2	7.8	9.4	8.0	6.3	5.1
26.971	5.1	6.9	7.5	9.7	8.8	5.6	5.2
27.086	6.0	10.6	11.5	10.4	8.0	6.7	4.9
27.202	6.2	14.3	16.1	12.0	9.9	4.8	5.0

Unexpectedly large false alarm rates experienced on some radars may be caused by this phenomenon.

The simulation of clutter and clutter spectral characteristics during anomalous propagation can be useful in handling these problems. Simulation of anomalous-propagation clutter can help distinguish unavoidable anomalous-propagation clutter from radar malfunction. For sites with frequent or severe anomalous propagation conditions, prediction of anomalous propagation clutter can influence site placement and operating parameters to mitigate the effect of those conditions. These APL clutter simulations are successfully factored into the Technical and Operational Evaluation of several radars used worldwide. They are helping us to understand peculiar radar system behavior caused by the anomalous propagation phenomenon, and are leading to new processing techniques and on-site procedures to cope with it.

REFERENCES

[1] H. W. Ko, J. W. Sari, and J. P. Skura, "Anomalous Microwave Propagation Through Atmospheric Ducts," *Johns Hopkins APL Tech. Dig.* **4**, 12–16 (1983).

[2] J. P. Skura, J. W. Sari, and H. W. Ko, "Application of the Parabolic Equation Method to Propagation in Inhomogeneous Refractive Layers," in *Proc. VRSI National Radio Science Meeting*, Boulder, Colo., p. 23 (1982).

[3] R. P. Wasky, "A Geometric Optics Model for Calculating the Field Strength of Electromagnetic Waves in the Presence of a Tropospheric Duct," MS Thesis, University of Dayton, Ohio (1977).

[4] M. I. Skolnik, *Radar Handbook*, McGraw-Hill, New York, pp. 25–28 (1970).

[5] P. J. Kahrilas, *Electronic Scanning Radar Systems Design Handbook*, Artech House, Needham, Mass., 155–156 (1976).

[6] J. P. Skura, "Worldwide Anomalous Refraction and its Effects on Electromagnetic Wave Propagation," *Johns Hopkins APL Tech. Dig.* **8**, 418–425 (1987).

[7] O. M. Phillips, *The Dynamics of the Upper Ocean*, Cambridge University Press, London, pp. 183–186 (1969).

[8] H. Medwin, C. S. Clay, J. M. Berkson, and D. Jaggard, "Traveling Correlation Function of the Height of Wind-Blown Water Waves," *J. Geophys. Res.* **75**, 4519–4524 (1970).

[9] A. W. Bjerkaas and F. W. Riedel, *Proposed Model for the Elevation Spectrum of a Wind Roughened Sea Surface*, JHU/APL TG 1328 (1979).

[10] D. J. Northam, *A Stochastic Simulation of Low Grazing Angle Forward Scatter Over Water Multipath Effects*, NRL Report 8568 (1981).

[11] K. L. Musser, "Radar Signal Processing Simulation," JHU/APL F3A-86-153 (1986).

ACKNOWLEDGMENTS—The authors would like to thank J. P. Skura and H. W. Ko for their suggestions and guidance concerning the development of this modeling system.

THE AUTHORS

SUSAN C. LEE was born in San Diego in 1952. She received a B.S. in physics from Duke University in 1973 and joined APL the same year. In 1978 she received an M.S. in computer science from The Johns Hopkins University Whiting School of Engineering. She received an M.S. in Technology Management from the Whiting School of Engineering in 1987.

At APL, Mrs. Lee has worked in the Space Department on the SAS-C, TIP, AMPTE, and TOPEX satellites. She also worked in the Submarine Technology Magnetics Group on several at-sea exercises. Her work is in software systems engineering.

DONALD E. MAURER is a mathematician in APL's Fleet Systems Department. He holds a B.A. from the University of Colorado and a Ph.D. from the California Institute of Technology. Dr. Maurer is a member of the American Mathematical Society, the New York Academy of Sciences, and the Society of Sigma Xi. He has worked as a mathematician at the Institute for Defense Analyses and the Center for Naval Analyses. His work now involves projects for modeling radar propagation and electromagnetic scattering from statistically rough surfaces.

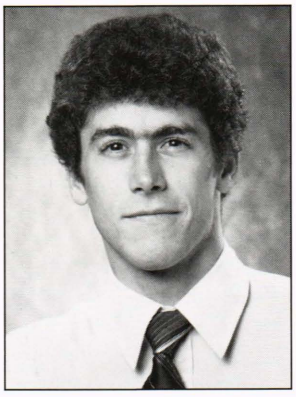

KEITH L. MUSSER was born in La Ronge, Saskatchewan, in 1964. He received a B.S. degree in electrical engineering from LeTourneau College in 1986. An associate engineer in APL's Spacecraft Guidance and Control Group, he is also a master's degree candidate at The Johns Hopkins University Whiting School of Engineering. Mr. Musser is a member of the IEEE Control Systems Society.